Nano Research 2018, 11(2): 1124–1134
https://doi.org/10.1007/s12274-017-1731-z
Research Article
ISSN 1998-0124
CN 11-5974/O4

CVD growth of fingerprint-like patterned 3D graphene film for an ultrasensitive pressure sensor

Kailun Xia, Chunya Wang, Muqiang Jian, Qi Wang, and Yingying Zhang (✉)

Key Laboratory of Organic Optoelectronics and Molecular Engineering of the Ministry of Education, Department of Chemistry and Center for Nano and Micro Mechanics (CNMM), Tsinghua University, Beijing 100084, China

Received: 26 April 2017
Revised: 11 June 2017
Accepted: 17 June 2017

KEYWORDS
electronic skin,
flexible pressure sensor,
three-dimensional (3D) graphene film,
fingertip skin,
hierarchical structures

ABSTRACT

With the rapid development of wearable devices, flexible pressure sensors with high sensitivity and wide workable range are highly desired. In nature, there are many well-adapted structures developed through natural selection, which inspired us for the design of biomimetic materials or devices. Particularly, human fingertip skin, where many epidermal ridges amplify external stimulations, might be a good example to imitate for highly sensitive sensors. In this work, based on unique chemical vapor depositions (CVD)-grown three-dimensional (3D) graphene films that mimic the morphology of fingertip skin, we fabricated flexible pressure sensing membranes, which simultaneously showed a high sensitivity of 110 $(kPa)^{-1}$ for 0–0.2 kPa and wide workable pressure range (up to 75 kPa). Hierarchical structured polydimethylsiloxane (PDMS) films molded from natural leaves were used as the supporting elastic films for the graphene films, which also contribute to the superior performance of the pressure sensors. The pressure sensor showed a low detection limit (0.2 Pa), fast response (< 30 ms), and excellent stability for more than 10,000 loading/unloading cycles. Based on these features, we demonstrated its applications in detecting tiny objects, sound, and human physiological signals, showing its potential in wearable electronics for health monitoring and human/machine interfaces.

1 Introduction

Electronic skin (e-skin) is of paramount importance for applications such as health monitoring, robotics, and prosthetics control, motivating a revolution in the field of electronics [1–8]. As a vital component of e-skin, flexible pressure sensors, which are highly sensitive and can be conformally attached on arbitrary surfaces, play critical roles in the development of e-skin [9–15]. The mechanisms of pressure sensors are typically based on transistor sensing [16], capacitive sensing [17–20], triboelectric sensing [21], piezoelectric sensing [22, 23], and piezo-resistive sensing [24–28], among which, the piezo-resistive pressure sensors have attracted increasing attention due to their simplicity in device fabrication and high sensitivity [29–32]. The

Address correspondence to yingyingzhang@tsinghua.edu.cn

typical strategy to fabricate a piezo-resistive pressure sensor is to combine conductive materials including nanowires [26, 32], carbon nanotubes [33–35], carbonized fabrics/film [36, 37], and graphene [16, 34, 38] with a flexible elastomer to obtain highly sensitive and flexible pressure sensors [30, 39–43].

Since its discovery in 2004 [44], graphene, as the star of two-dimensional (2D) materials, has gained extensive attention [45, 46]. Due to its high transmittance, superior electron mobility, high electrical and thermal conductivity, and excellent mechanical flexibility, significant efforts have focused on the applications of carbon materials in flexible electronic devices [47], including flexible displays [48], energy devices [49, 50], and flexible sensors [51–53]. Particularly, graphene can be used for the fabrication of flexible pressure sensors. With an external force loading, the symmetry of the atomic periodicity in graphene will break, and the electronic structure will distort, inducing piezo-resistive responses. Although the flexibility of graphene pressure sensors is excellent, the response of pristine graphene to pressure is relatively small, indicating a low sensitivity. In order to increase the sensitivity, various strategies using structured graphene or patterned substrates have been developed. For example, hierarchical structured polydimethylsiloxane (PDMS) covered with a graphene monolayer has been used to fabricate a pressure sensor, which showed a sensitivity of 8.5 $(kPa)^{-1}$ in a pressure range of 0–12 kPa and detection limit of 1 Pa [54]. A bubble-decorated honeycomb like graphene film was used to fabricate a pressure sensor, which showed a sensitivity of 161.6 $(kPa)^{-1}$ for the pressure ranges of 9–560 Pa and 0.92 $(kPa)^{-1}$ for 2–10 kPa [29]. In addition, graphene self-assembled in a porous polymer sponge, such as a polyurethane sponge, have also been reported as pressure sensors [55, 56]. Despite these great achievements, it is still challenging to fabricate graphene pressure sensors with both high sensitivity and wide pressure sensing range. The morphology and structure of the graphene in the pressure sensor play vital roles in determining the performance. Clearly, hierarchical structures in both the active graphene materials and supporting matrix will promote the performance of the pressure sensors. Actually, there are many hierarchical structures in nature that have developed after the millions of years of natural selection, inspiring us to develop bio-mimicking materials and systems with superior performances. Particularly, there are many epidermal ridges on the skin of the human fingertip, which serve to amplify subtle external stimulations, inspiring us to design highly sensitive fingertip-skin like pressure sensors.

Here, we report the growth of a three-dimensional (3D) graphene film mimicking the morphology of fingertip-skin directly by chemical vapor deposition (CVD) and demonstrated its application in highly sensitive flexible pressure sensors with a wide response range. The 3D graphene film, which consists of a continuous graphene film and closely packed concentric graphene nanoribbon rings, formed from the fast growth of graphene in a CVD system with abundant gas precursors and H_2. To achieve ultrasensitive pressure sensors, hierarchical structured PDMS films, which were molded from natural leaves, were used as the supporting films, endowing abundant contact sites for improving the sensitivity. Pressure sensors were fabricated by integrating the 3D graphene film with hierarchical structured flexible elastomer substrates, which showed sensitivity of 110 $(kPa)^{-1}$ for a pressure range of 0–0.2 kPa, 3 $(kPa)^{-1}$ within 0.2–15 kPa, and 0.26 $(kPa)^{-1}$ for a pressure range of 15–75 kPa. Based on the superior performance of the pressure sensor, we demonstrated its applications in detecting tiny objects, sound, and human physiological signals including wrist pulse and throat phonation signals, showing its wide potential applications in wearable devices, human-machine interfacing, and smart robots.

2 Results and discussion

The 3D graphene film was synthesized on a Cu substrate using atmospheric pressure CVD. The growth of fingerprint-like 3D graphene film was carried out with a high partial pressure of hydrogen (H_2) and methane (CH_4) (see Experimental). The key parameter in the formation of concentric hexagonal graphene nanoribbon rings in the 3D graphene film is the large partial pressure of H_2. Figure 1(a) illustrates the growth process and the proposed growth mechanism of the 3D graphene film. The growth process can be summarized as the repeated nucleation, growth,

and coalescence of graphene seeds, forming the 3D structure. During the traditional 2D graphene growth process, graphene nucleates on the active sites (such as impurities, sharp wrinkles, and defects) on the Cu surface, and then grows by capturing the carbon species [56]. In contrast, the formation mechanism of the fingerprint-like 3D graphene is different from the seed-induced 2D graphene growth, which can be regarded as edge-nucleated. Firstly, monolayer graphene domains nucleate on the Cu surface and constantly grow by capturing active carbon species. With the formation of the upper graphene layer, new graphene layers will nucleate under the edge of the initial graphene layer and then form multi-layer graphene nanoribbons, which can be understood considering the edge seed-induced growth occurred in a hydrogen rich environment [57–59]. At the same time, the top layer graphene continues to grow and exposes new edges for nucleation. Because the top graphene film grows faster than the new graphene layers underneath, the top layer of graphene repeatedly exposes new edges, eventually forming concentric graphene nanoribbon rings beneath the top graphene film. Figure 1(b) schematically illustrates the structure of a 3D graphene film, which contains a continuous graphene film and closely packed concentric hexagonal graphene nanoribbon rings. The unique structure endowed the graphene film with excellent electrical conductivity, structural integrity, and high potential for applications in sensors. The structure of the 3D graphene film was similar to the morphology of fingertip skin (Fig. 1(c)), where connected epidermal ridges amplify subtle stimulation.

Figure 1(d) shows the scanning electron microscope (SEM) image of a 3D graphene film transferred onto a silicon (Si) substrate with a 285-nm thick silicon oxide

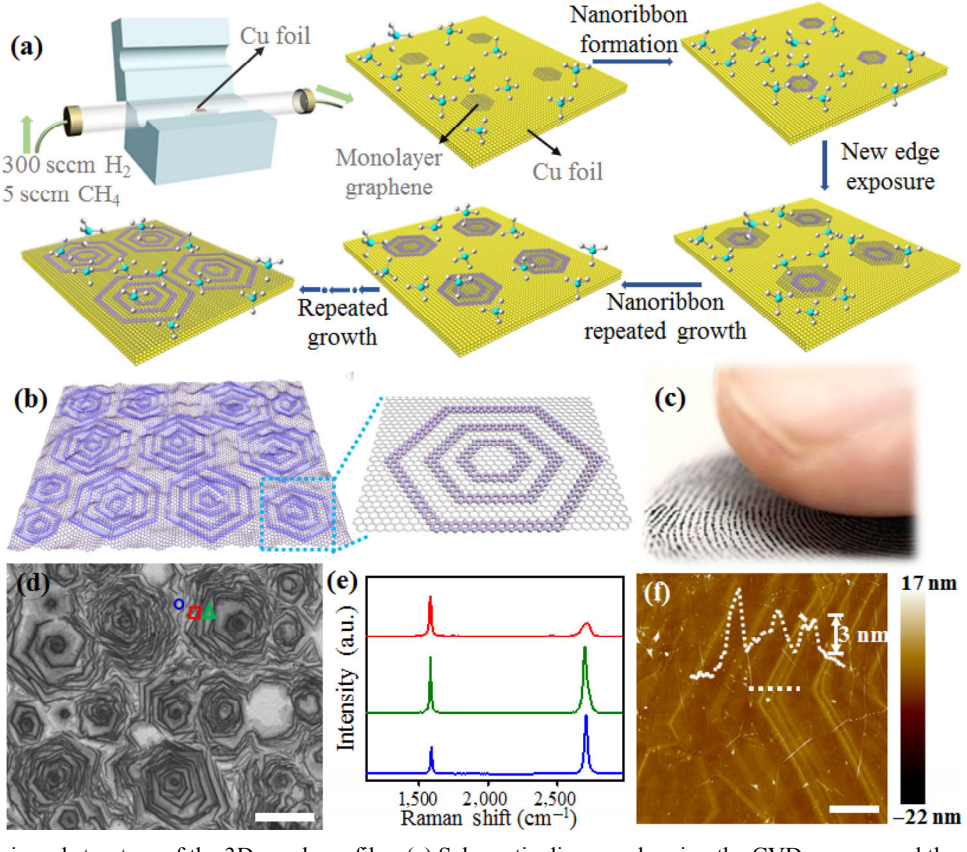

Figure 1 Synthesis and structure of the 3D graphene film. (a) Schematic diagram showing the CVD process and the mechanism for the growth of 3D graphene film. (b) Schematic illustration showing the structure of the 3D graphene film containing a continuous graphene film and closely packed concentric hexagonal graphene nanoribbon rings. (c) Picture of a fingertip and its fingerprint. (d) SEM image of a 3D graphene film on a SiO_2/Si substrate. Scale bar: 20 μm. (e) Raman spectra taken from three points of a graphene domain in (d). The top line corresponds to the darker area indicated by the square and the bottom line corresponds to the lighter area indicated by the circle. (f) AFM image taken from a part of a graphene domain. The inset line shows the height of the graphene ribbons. Scale bar: 5 μm.

layer (SiO_2). The color contrast shows the different thicknesses of the graphene film. The graphene nanoribbon rings with dark color were uniformly arranged around the nucleation centers, forming concentric structures. Raman spectroscopy was used to further characterize the 3D graphene film. Raman spectra obtained from three points in one graphene domain are shown in Fig. 1(e). The top layer of graphene was composed of a monolayer and few-layered graphene domains, and the graphene nanoribbon rings had relatively more layers of graphene. In Fig. 1(d), for the point with a circle, the intensity ratio of the 2D peak to G peak (I_{2D}/I_G) was larger than 2, and the full width at half-maximum of the 2D peak was about 30 cm^{-1}, indicating it was a monolayer graphene domain. In contrast, for the area marked with a triangle, the I_{2D}/I_G was near 1, indicating it was a few-layered graphene domain, and for the area marked with a square, the I_{2D}/I_G of the Raman spectrum was much smaller than 1, indicating there was multilayer graphene. We further used atomic force microscopy (AFM) to characterize the morphology of a 3D graphene film that was transferred onto a 285 nm SiO_2/Si substrate. Figure 1(f) shows the AFM image taken from a part of a graphene domain. Closely packed concentric graphene nanoribbon rings with an intersection angle of 120° can clearly be observed. As shown by the section analysis, the height of the graphene nanoribbon was around 3–5 nm, demonstrating the unique 3D structure of the graphene film.

To fabricate high performance pressure sensors, the 3D graphene film was combined with hierarchical structured elastic substrates. Flexible substrates containing uniform microstructures can promote the sensitivity of the pressure sensor for small pressures. However, this strategy is not effective for large pressures, leading to a limited detecting pressure range [27]. Natural plant leaves possess unique hierarchical structures, including macroscale veins and surface micro/nano-structures. Figure 2(a) schematically illustrates the assembling process of a pressure sensor based on 3D graphene films and hierarchical structured PDMS films. The PDMS films were molded from *Epipremnum aureum* leaves. The thickness of the PDMS film was controlled within a range of 280 ± 50 μm. The surface structures of the leaf and the PDMS film were characterized using optical microscopy, SEM, and AFM. As shown in Figs. 2(b) and 2(c), there are dense small protuberances located on large embossments on the *E. aureum* leaf. Figure 2(d) shows the morphology

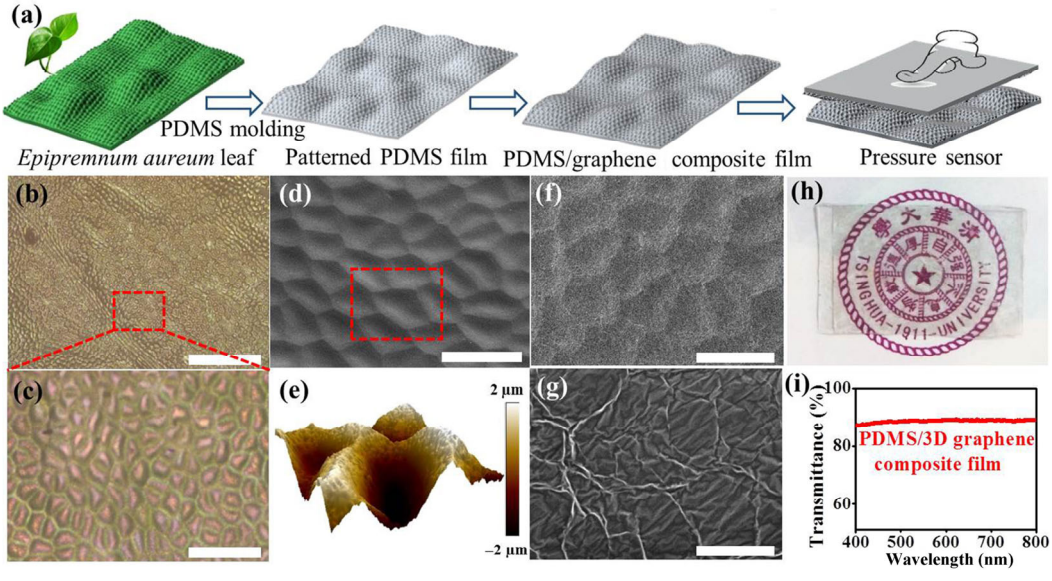

Figure 2 Fabrication process of the pressure sensors and the hierarchical structures of the films. (a) Schematic illustration showing the fabrication process of a pressure sensor. (b) and (c) Optical images of an *E. aureum* leaf. Scale bar in (b): 500 μm and scale bar in (c): 100 μm. (d) SEM image of a patterned PDMS film. Scale bar: 50 μm. (e) 3D view AFM image of a patterned PDMS film. (f) and (g) SEM images of a patterned PDMS thin film covered with a 3D graphene film. Scale bar in (f): 50 μm and scale bar in (g): 2 μm. (h) Photograph of a flexible pressure sensor. (i) Transmittance spectra of the PDMS/graphene composites film.

of the molded PDMS film, indicating the structures on the leaf can be transferred onto the PDMS film with good fidelity. Figure 2(e) shows a 3D AFM image of the PDMS film, demonstrating the convex polygonal structures with a height of about 4 μm. Figures 2(f) and 2(g) exhibit typical SEM images of the patterned PDMS film covered with a 3D graphene film, showing the conformal coating of the graphene on the PDMS surface, which is of great importance to achieve pressure sensors with high stability. In addition, the PDMS/graphene composite films have high transmittance near 90%, as shown in Figs. 2(h) and 2(i). Finally, an interlocked construction pressure sensor was constructed by putting two PDMS/graphene composite films face to face while using two Cu wires connected to each of the two films as the electrodes.

The bionic hierarchical structures in the pressure sensor endowed it with high sensitivity within a wide pressure range. Figure 3(a) schematically illustrates the evolution of the contact between the top and bottom hierarchical structured composite films with a pressure loading. As the external pressure increases, the hierarchical structures on the surface will deform and the number of contact points will increase. Figure 3(b) shows the current-pressure plot of the pressure sensor. The sensitivity (S) of the pressure sensor can be defined as

$$S = \frac{\frac{I - I_0}{I_0}}{P - P_0} \quad (1)$$

where I_0 is the initial current of the pressure sensor, I is the current of the pressure sensor with the application of external pressure, and P is the applied pressure. As shown in Fig. 3(b), the curve can be divided into three parts according to the sensitivity. The sensitivity was 110 $(kPa)^{-1}$ for a pressure range of 0–0.2 kPa, 3 $(kPa)^{-1}$ in a pressure range of 0.2–15 kPa, and 0.26 $(kPa)^{-1}$ for 15–75 kPa and even higher pressure. We compared the performance of different devices and found that the 3D graphene film based pressure sensors showed good uniformity and repeatability (Fig. S1 in the Electronic Supplementary Material (ESM)). Under static pressure, the sensors showed steady responses, and the signals remained constant under each static pressure (Fig. S2 in the ESM). Figure 3(c) presents the cyclic response of the device to some fixed small pressures in the range of 15–250 Pa, indicating the excellent stability of the pressure sensor for monitoring small pressures. Furthermore, we increased the loading/unloading frequency from 0.5 to 2 Hz and found the corresponding signals remained steady without any observable variations (Fig. S3 in the ESM), indicating the fast response and instant recovery of the pressure sensor. Figure 3(d) shows the response time of the sensor, which is less than 30 ms. Figure 3(e) shows the responses of the device to cyclic loading/unloading of a pressure of 150 Pa for more than 10,000 cycles. Furthermore, the results showing cyclic loading/unloading of 70 kPa for more than 5,000 cycles are shown in Fig. S4 in the ESM. These results reveal that the pressure sensor possessed high stability, good repeatability, and excellent durability with unobservable hysteresis.

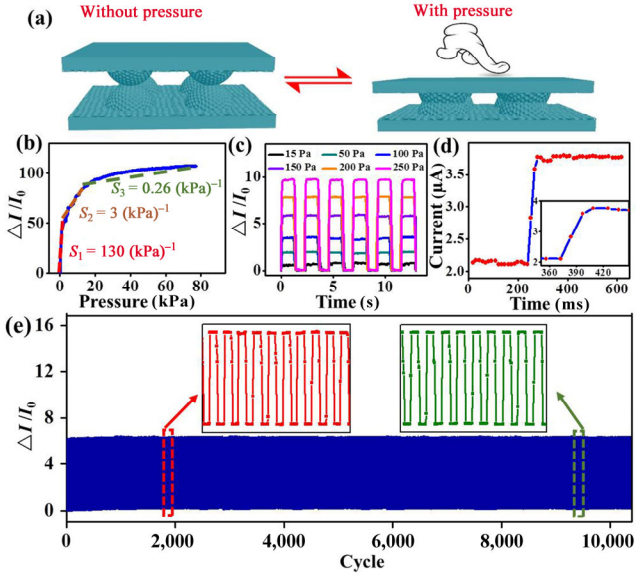

Figure 3 Performance of the bionic hierarchical structured pressure sensor based on 3D graphene films. (a) Schematic illustration showing the contact phenomena of hierarchical structured PDMS/graphene composites film with pressure. (b) Current–pressure plot for pressure range of 0–75 kPa. The sensitivity is 110 $(kPa)^{-1}$ within 0–0.2 kPa, 3 $(kPa)^{-1}$ in a pressure range of 0.2–15 kPa, and 0.26 $(kPa)^{-1}$ for 15–75 kPa and even higher pressure. (c) Current–pressure plots of the pressure sensor obtained with cyclic loading–unloading of certain small pressures. (d) Response time of the pressure sensor for 50 Pa, showing its fast response within 30 ms. (g) Cyclic loading/unloading test under 150 Pa for 10,000 cycles. The applied voltage is 3 V in all tests.

To confirm the contribution of the unique fingerprint-like 3D graphene structure to the performance of the pressure sensors, we also fabricated a pressure sensor using plain monolayer graphene films coated on hierarchical structured PDMS films for comparison. When monolayer graphene was used, the pressure sensor showed relatively low sensitivity (Fig. S5 in the ESM) and low stability compared to that of the 3D graphene pressure sensor. Under physical deformations, cracks more easily form in plain monolayer graphene films, resulting in unstable performance. These results revealed the vital role of the fingerprint-like 3D graphene film on ensuring the high performance of the pressure sensors. In addition, we further explored the influence of temperature and humidity on the sensor. The sensor was tested with loadings of 100 and 1,000 Pa at a temperature range of 10 to 90 ℃, and it exhibited only slight signal drift with temperature (Fig. S6(a) in the ESM). As for the influence of humidity, we sprayed water vapor on the sensor while loading a grain of mung beans on it and found that the response of the sensor remained stable (Fig. S6(b) in the ESM). We compared the performance of our pressure sensor with reported representative high-performance, flexible, piezo-resistive pressure sensors and summarized the results in Table S1 in the ESM. The bionic hierarchical structured pressure sensor based on 3D graphene films possessed superior performance including high sensitivity, low detection limit, and fast response, promising great potential in applications for wearable devices.

To confirm the contribution of the hierarchical structures on the PDMS films to the performance of the pressure sensors, we also fabricated a pressure sensor using PDMS films molded from a Teflon membrane for comparison. The film molded from the Teflon membrane only had smaller microstructures on the surface, which were dense bulges with a size of 500 nm and height of 1 μm (Fig. S7 in the ESM). The testing results showed that the pressure sensor with structures molded from the Teflon membrane had relatively low sensitivity and limited workable pressure range (Fig. S8 in the ESM), indicating the importance the hierarchical structures on the PDMS films molded from the natural *E. aureum* leaf in determining the performance of the pressure sensors.

Owing to its high sensitivity and wide workable pressure range, the flexible pressure sensors based on 3D graphene films have many potential applications in wearable electronics. We demonstrated its application in detection of subtle pressures. Figures 4(a)–4(c) showed the response of the pressure sensor to tiny objects, including a piece of paper, a pupa, and staples. As seen in Fig. 4(a), the pressure sensor can detect the loading of a piece of paper with a weight of only 8 mg (about 0.2 Pa), showing a detection limit lower than many previous reports [24, 26–28].

In addition, subtle human motions, including pulse and phonation could also be accurately and promptly detected by the 3D graphene film based bionic pressure sensor. For demonstration, we attached a pressure sensor on the wrist of a volunteer (as seen in Fig. 4(d)). Figure 4(e) shows the current variation induced by the pulse in a relaxed state and after exercise. The results clearly demonstrated the stable and repeatable pulse shape in a relaxed condition with a frequency of 78 beats per minute and the deformed shape after exercise with a frequency of 126 beats per minute. A typical magnified pulse waveform obtained in the relaxed condition is shown in Fig. 4(f), clearly displaying the percussion wave (P-wave), tidal wave (T-wave) and dicrotic wave (D-wave) that are related to the systolic and diastolic blood pressure, the ventricular rate, and the heart rate, respectively. These results show that the potential of the pressure sensor as a non-invasive medical device for monitoring human health in real time.

The device could also be attached onto a neck to monitor tiny muscle and epidermal movement during speaking to recognize phonation, as shown in Fig. 4(g). Figures 4(h)–4(j) show the detected current change signals during the subject repeatedly saying "hello", "carbon", and "graphene", respectively, displaying distinguishable and repeatable signal patterns corresponding to specific words. Sounds could also be detected by the pressure sensor. A pressure sensor based on the 3D graphene film was attached on the vibrating membrane of a loudspeaker box, which was playing repeated audio (Fig. S9(a) in the ESM), and the signal of the sensor corresponding

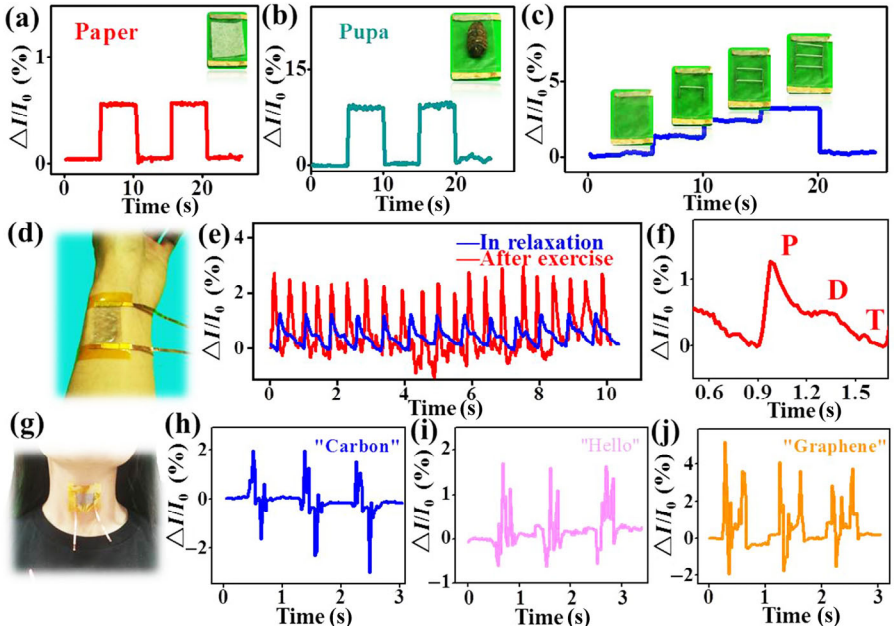

Figure 4 Applications of the pressure sensor in detection of tiny objects and subtle human motions. (a)–(c) Response signals induced by loading of (a) a piece of paper, (b) a pupa, and (c) staples. (d) Photograph showing a sensor attached onto a wrist. (e) Signals induced by a pulse in a relaxed state and after exercise. (f) Magnified pulse waveform. (g) Photograph of a pressure sensor attached on a neck. (h)–(j) Signals induced by speaking of (h) "carbon", (i) "hello", and (j) "graphene".

to the played audio is shown in Fig. S9(b) in the ESM. The sensor showed an almost synchronous response to the audio and most of the characteristic peaks remained consistent during the loop playback, demonstrating the potential application of the pressure sensor in phonation rehabilitation training and human/machine interaction.

For practical applications in wearable devices and e-skin, the spatially resolved detection of pressures is highly desired. We fabricated a pressure sensor matrix with 64 pixels (8 × 8 elements) using large-area 3D graphene films as the active materials (as seen in Fig. S10(a) in the ESM). When touched by a fingertip, the sensor array displayed a current change signal mapping (Fig. S10(b) in the ESM) corresponding to the distribution of pressures on the surface. We also loaded small glass beads on the sensor array to see its response (Figs. S10(c) and S10(d) in the ESM), demonstrating its ability for spatial resolution.

3 Conclusions

In summary, we reported the direct growth of fingerprint-like patterned 3D graphene films by CVD. Using these films, we fabricated high performance wearable pressure sensors with high sensitivity in a wide workable pressure range. Two 3D graphene films individually supported on a hierarchical structured PDMS film were put face to face and fabricated into a pressure sensor with good flexibility and transparency. The bionic hierarchical structures in the pressure sensor endow it with both a superior sensitivity and wide workable range. The pressure sensor shows sensitivity as high as 110 $(kPa)^{-1}$ (for 0–0.2 kPa), fast response (< 30 ms), high durability, and a detection limit as low as 0.2 Pa. Based on its high performance, we demonstrated its applications in detecting tiny objects, subtle human physiological signals (such as wrist pulses and phonation), and sounds. Furthermore, the 3D graphene films could be easily fabricated into a sensor array for spatially resolved detection of pressures. We believe this bionic graphene pressure sensor, based on its high performance and facile fabrication, might have great potential in health monitoring, voice discrimination, phonation rehabilitation training, and human/machine interfaces.

4 Experimental

4.1 Synthesis of the 3D graphene film

The 3D graphene film was directly grown on copper foil (25 μm thick, Alfa Aesar Inc) by CVD. The copper foil was cleaned in acetic acid for 30 min at 80 ˚C to remove the surface oxide and then washed with acetone, ethyl alcohol, and deionized (DI) water. After being dried in nitrogen, the copper foil was put in a high-temperature tube furnace and heated to 1,060 ˚C in 60 min with a flow of argon (250 sccm, 99.999% purity). After the temperature reached 1,060 ˚C, 300 sccm hydrogen (99.999% purity) was introduced into the system and maintained for 1 h. The growth of the 3D graphene film was carried out with the introduction of methane (5 sccm, 99.999% purity) for several minutes. The growth was terminated by stopping the methane flow and cooling down the system in argon and hydrogen.

4.2 Transfer of graphene to target substrates

The transfer process was as follows: (1) Coating PMMA on the surface of the graphene/copper sample by spin coating (3,000 rpm for 30 s), (2) heating at 180 ˚C for 30 min, (3) etching the copper in 1 mol/L $FeCl_3$/HCl solution, (4) cleaning the floating graphene/PMMA films three times with DI water, (5) picking up the graphene/PMMA films with target substrates, (6) drying for 1 h in a blast oven, (7) dissolving the PMMA layer using 60 ˚C acetone, and (8) removing the remaining acetone in the blast oven for 10 min.

4.3 Characterization of the 3D graphene film

The structure of the 3D graphene films was characterized by an optical microscope (LEICA DM2500 M), an AFM (NanoScope V, Veeco), and a field emission scanning electron microscope (FE-SEM) (FEI Quanta 650). The quality and layer numbers of the graphene was characterized by a Raman spectroscope with a laser excitation wavelength of 532 nm.

4.4 Preparation of hierarchical structured PDMS film

First, *E. aureum* leaves were chosen and cleaned with DI water. Then, these leaves were blow dried and fixed on the flat surface of petri dish with double-sided adhesive tape. Polydimethylsiloxane (Sylgard184) precursor with a curing agent in a 10:1 ratio by weight was prepared and poured onto the leaves, followed by heating at 80 ˚C for 3 h. Finally, hierarchical structured PDMS films were obtained by peeling the film off.

4.5 Fabrication and testing of the flexible pressure sensor

The flexible pressure sensor was constructed with hierarchical structured PDMS films covered with 3D graphene films. On each of the PDMS/graphene composite films, a copper wire was attached at the side to work as the electrode. The flexible pressure sensor was fabricated by placing two PDMS/graphene composite films face to face. The loading of pressure was performed with a universal testing machine (SHIMADZU AGS-X), while the current signals of the pressure sensor were recorded using a digital meter (Keithley 2400). To fabricate the pressure sensor matrix with 64 pixels (8 × 8 elements), two pieces of 3D graphene/elastomer films with an area of 50 mm × 50 mm were used and the interspaces between each 3 mm × 3 mm pixel were formed by partially removing the 3D graphene films through scotch tape. The electrical response of the pressure sensor was tested using a digital meter (Keithley 2400).

Acknowledgements

This work was supported by the National Natural Science Foundation of China (NSFC) (Nos. 51422204, 51672153 and 51372132) and the National Basic Research Program of China (973 Program) (Nos. 2016YFA0200103 and 2013CB228506).

Electronic Supplementary Material: Supplementary material (supplementary figures (Figs. S1–S10) and supplementary texts about CVD growth of fingerprint-like patterned 3D graphene film for ultrasensitive pressure sensor) is available in the online version of this article at https://doi.org/10.1007/s12274-017-1731-z.

References

[1] Trung, T. Q.; Ramasundaram, S.; Hwang, B. U.; Lee, N. E.

An all-elastomeric transparent and stretchable temperature sensor for body-attachable wearable electronics. *Adv. Mater.* **2016**, *28*, 502–509.

[2] Windmiller, J. R.; Wang, J. Wearable electrochemical sensors and biosensors: A review. *Electroanalysis* **2013**, *25*, 29–46.

[3] Shaplov, A. S.; Ponkratov, D. O.; Aubert, P. H.; Lozinskaya, E. I.; Plesse, C.; Vidal, F.; Vygodskii, Y. S. A first truly all-solid state organic electrochromic device based on polymeric ionic liquids. *Chem. Commun.* **2014**, *50*, 3191–3193.

[4] Lipomi, D. J.; Tee, B. C. K.; Vosgueritchian, M.; Bao, Z. N. Stretchable organic solar cells. *Adv. Mater.* **2011**, *23*, 1771–1775.

[5] Kim, Y.; Zhu, J.; Yeom, B.; Di Prima, M.; Su, X. L.; Kim, J. G.; Yoo, S. J.; Uher, C.; Kotov, N. A. Stretchable nanoparticle conductors with self-organized conductive pathways. *Nature* **2013**, *500*, 59–63.

[6] Ahn, J. H.; Je, J. H. Stretchable electronics: Materials, architectures and integrations. *J. Phys. D Appl. Phys.* **2012**, *45*, 103001.

[7] Lee, J.; Lee, P.; Lee, H. B.; Hong, S.; Lee, I.; Yeo, J.; Lee, S. S.; Kim, T. S.; Lee, D.; Ko, S. H. Room-temperature nanosoldering of a very long metal nanowire network by conducting-polymer-assisted joining for a flexible touch-panel application. *Adv. Funct. Mater.* **2013**, *23*, 4171–4176.

[8] Rogers, J. A.; Someya, T.; Huang, Y. G. Materials and mechanics for stretchable electronics. *Science* **2010**, *327*, 1603–1607.

[9] Wang, C.; Hwang, D.; Yu, Z. B.; Takei, K.; Park, J.; Chen, T.; Ma, B. W.; Javey, A. User-interactive electronic skin for instantaneous pressure visualization. *Nat. Mater.* **2013**, *12*, 899–904.

[10] Takei, K.; Takahashi, T.; Ho, J. C.; Ko, H.; Gillies, A. G.; Leu, P. W.; Fearing, R. S.; Javey, A. Nanowire active-matrix circuitry for low-voltage macroscale artificial skin. *Nat. Mater.* **2010**, *9*, 821–826.

[11] Mannsfeld, S. C. B.; Tee, B. C. K.; Stoltenberg, R. M.; Chen, C. V. H. H.; Barman, S.; Muir, B. V. O.; Sokolov, A. N.; Reese, C.; Bao, Z. N. Highly sensitive flexible pressure sensors with microstructured rubber dielectric layers. *Nat. Mater.* **2010**, *9*, 859–864.

[12] Schwartz, G.; Tee, B. C. K.; Mei, J. G.; Appleton, A. L.; Kim, D. H.; Wang, H. L.; Bao, Z. N. Flexible polymer transistors with high pressure sensitivity for application in electronic skin and health monitoring. *Nat. Commun.* **2013**, *4*, 1859.

[13] Kim, D. H.; Lu, N. S.; Ma, R.; Kim, Y. S.; Kim, R. H.; Wang, S. D.; Wu, J.; Won, S. M.; Tao, H.; Islam, A. et al. Epidermal electronics. *Science* **2011**, *333*, 838–843.

[14] Ghosh, S. K.; Adhikary, P.; Jana, S.; Biswas, A.; Sencadas, V.; Gupta, S. D.; Tudu, B.; Mandal, D. Electrospun gelatin nanofiber based self-powered bio-e-skin for health care monitoring. *Nano Energy* **2017**, *36*, 166–175.

[15] Lee, S.; Reuveny, A.; Reeder, J.; Lee, S.; Jin, H.; Liu, Q. H.; Yokota, T.; Sekitani, T.; Isoyama, T.; Abe, Y. et al. A transparent bending-insensitive pressure sensor. *Nat. Nanotechnol.* **2016**, *11*, 472–478.

[16] Hou, C. Y.; Wang, H. Z.; Zhang, Q. H.; Li, Y. G.; Zhu, M. F. Highly conductive, flexible, and compressible all-graphene passive electronic skin for sensing human touch. *Adv. Mater.* **2014**, *26*, 5018–5024.

[17] Cohen, D. J.; Mitra, D.; Peterson, K.; Maharbiz, M. M. A highly elastic, capacitive strain gauge based on percolating nanotube networks. *Nano Lett.* **2012**, *12*, 1821–1825.

[18] Gao, Q.; Meguro, H.; Okamoto, S.; Kimura, M. Flexible tactile sensor using the reversible deformation of poly(3-hexylthiophene) nanofiber assemblies. *Langmuir* **2012**, *28*, 17593–17596.

[19] Jung, S.; Lee, J.; Hyeon, T.; Lee, M.; Kim, D. H. Fabric-based integrated energy devices for wearable activity monitors. *Adv. Mater.* **2014**, *26*, 6329–6334.

[20] Nie, B. Q.; Li, R. Y.; Cao, J.; Brandt, J. D.; Pan, T. R. Flexible transparent iontronic film for interfacial capacitive pressure sensing. *Adv. Mater.* **2015**, *27*, 6055–6062.

[21] Yang, Y.; Zhang, H. L.; Lin, Z. H.; Zhou, Y. S.; Jing, Q. S.; Su, Y. J.; Yang, J.; Chen, J.; Hu, C. G.; Wang, Z. L. Human skin based triboelectric nanogenerators for harvesting biomechanical energy and as self-powered active tactile sensor system. *ACS Nano* **2013**, *7*, 9213–9222.

[22] Zhou, J.; Gu, Y. D.; Fei, P.; Mai, W. J.; Gao, Y. F.; Yang, R. S.; Bao, G.; Wang, Z. L. Flexible piezotronic strain sensor. *Nano Lett.* **2008**, *8*, 3035–3040.

[23] Mandal, D.; Yoon, S.; Kim, K. J. Origin of piezoelectricity in an electrospun poly(vinylidene fluoride-trifluoroethylene) nanofiber web-based nanogenerator and nano-pressure sensor. *Macromol. Rapid Commun.* ***2011***, *32*, *831–837*.

[24] Pang, C.; Lee, G. Y.; Kim, T. I.; Kim, S. M.; Kim, H. N.; Ahn, S. H.; Suh, K. Y. A flexible and highly sensitive strain-gauge sensor using reversible interlocking of nanofibres. *Nat. Mater.* **2012**, *11*, 795–801.

[25] Yamada, T.; Hayamizu, Y.; Yamamoto, Y.; Yomogida, Y.; Izadi-Najafabadi, A.; Futaba, D. N.; Hata, K. A stretchable carbon nanotube strain sensor for human-motion detection. *Nat. Nanotechnol.* **2011**, *6*, 296–301.

[26] Gong, S.; Schwalb, W.; Wang, Y. W.; Chen, Y.; Tang, Y.; Si, J.; Shirinzadeh, B.; Cheng, W. L. A wearable and highly sensitive pressure sensor with ultrathin gold nanowires. *Nat. Commun.* **2014**, *5*, 3132.

[27] Choong, C. L.; Shim, M. B.; Lee, B. S.; Jeon, S.; Ko, D. S.; Kang, T. H.; Bae, J.; Lee, S. H.; Byun, K. E.; Im, J. et al. Highly stretchable resistive pressure sensors using a conductive elastomeric composite on a micropyramid array. *Adv. Mater.* **2014**, *26*, 3451–3458.

[28] Luo, N. Q.; Dai, W. X.; Li, C. L.; Zhou, Z. Q.; Lu, L. Y.; Poon, C. C. Y.; Chen, S. C.; Zhang, Y. T.; Zhao, N. Flexible piezoresistive sensor patch enabling ultralow power cuffless blood pressure measurement. *Adv. Funct. Mater.* **2016**, *26*, 1178–1187.

[29] Sheng, L. Z.; Liang, Y.; Jiang, L. L.; Wang, Q.; Wei, T.; Qu, L. T.; Fan, Z. J. Bubble-decorated honeycomb-like graphene film as ultrahigh sensitivity pressure sensors. *Adv. Funct. Mater.* **2015**, *25*, 6545–6551.

[30] Yao, H. B.; Ge, J.; Wang, C. F.; Wang, X.; Hu, W.; Zheng, Z. J.; Ni, Y.; Yu, S. H. A flexible and highly pressure-sensitive graphene–polyurethane sponge based on fractured microstructure design. *Adv. Mater.* **2013**, *25*, 6692–6698.

[31] Pan, L. J.; Chortos, A.; Yu, G. H.; Wang, Y. Q.; Isaacson, S.; Allen, R.; Shi, Y.; Dauskardt, R.; Bao, Z. N. An ultra-sensitive resistive pressure sensor based on hollow-sphere microstructure induced elasticity in conducting polymer film. *Nat. Commun.* **2014**, *5*, 3002.

[32] He, W. N.; Li, G. Y.; Zhang, S. Q.; Wei, Y.; Wang, J.; Li, Q. W.; Zhang, X. T. Polypyrrole/silver coaxial nanowire aero-sponges for temperature-independent stress sensing and stress-triggered joule heating. *ACS Nano* **2015**, *9*, 4244–4251.

[33] Trung, T. Q.; Lee, N. E. Flexible and stretchable physical sensor integrated platforms for wearable human-activity monitoringand personal healthcare. *Adv. Mater.* **2016**, *28*, 4338–4372.

[34] Jang, H.; Park, Y. J.; Chen, X.; Das, T.; Kim, M. S.; Ahn, J. H. Graphene-based flexible and stretchable electronics. *Adv. Mater.* **2016**, *28*, 4184–4202.

[35] Cheng, T.; Zhang, Y. Z.; Lai, W. Y.; Huang, W. Stretchable thin-film electrodes for flexible electronics with high deformability and stretchability. *Adv. Mater.* **2015**, *27*, 3349–3376.

[36] Wang, C. Y.; Li, X.; Gao, E. L.; Jian, M. Q.; Xia, K. L.; Wang, Q.; Xu, Z. P.; Ren, T. L.; Zhang, Y. Y. Carbonized silk fabric for ultrastretchable, highly sensitive, and wearable strain sensors. *Adv. Mater.* **2016**, *28*, 6640–6648.

[37] Zhang, M. C.; Wang, C. Y.; Wang, H. M.; Jian, M. Q.; Hao, X. Y.; Zhang, Y. Y. Carbonized cotton fabric for high-performance wearable strain sensors. *Adv. Funct. Mater.* **2017**, *27*, 1604795.

[38] Tian, H.; Shu, Y.; Wang, X. F.; Mohammad, M. A.; Bie, Z.; Xie, Q. Y.; Li, C.; Mi, W. T.; Yang, Y.; Ren, T. L. A graphene-based resistive pressure sensor with record-high sensitivity in a wide pressure range. *Sci. Rep.* **2015**, *5*, 8603.

[39] Chen, Z.; Wang, Z.; Li, X.;Lin, Y.; Luo, N.; Long, M.; Zhao, N.; Xu, J. B. Flexible piezoelectric-induced pressure sensors for static measurements based on nanowires/graphene heterostructures. *ACS Nano.* **2017**, *11*, 4507–4513.

[40] Wagner, S.; Bauer, S. Materials for stretchable electronics. *MRS Bull.* **2012**, *37*, 207–213.

[41] Park, M.; Im, J.; Shin, M.; Min, Y.; Park, J.; Cho, H.; Park, S.; Shim, M. B.; Jeon, S.; Chung, D. Y. et al. Highly stretchable electric circuits from a composite material of silver nano-particles and elastomeric fibres. *Nat. Nanotechnol.* **2012**, *7*, 803–809.

[42] Tang, Y.; Gong, S.; Chen, Y.; Yap, L. W.; Cheng, W. L. Manufacturable conducting rubber ambers and stretchable conductors from copper nanowire aerogel monoliths. *ACS Nano* **2014**, *8*, 5707–5714.

[43] Zhu, B. W.; Niu, Z. Q.; Wang, H.; Leow, W. R.; Wang, H.; Li, Y. G.; Zheng, L. Y.; Wei, J.; Huo, F. W.; Chen, X. D. Microstructured graphene arrays for highly sensitive flexible tactile sensors. *Small* **2014**, *10*, 3625–3631.

[44] Novoselov, K. S.; Geim, A. K.; Morozov, S. V.; Jiang, D.; Zhang, Y.; Dubonos, S. V.; Grigorieva, I. V.; Firsov, A. A. Electric field effect in atomically thin carbon films. *Science* **2004**, *306*, 666–669.

[45] Neto, A. H. C.; Guinea, F.; Peres, N. M. R.; Novoselov, K. S.; Geim, A. K. The electronic properties of graphene. *Rev. Mod. Phys.* **2009**, *81*, 109–162.

[46] Allen, M. J.; Tung, V. C.; Kaner, R. B. Honeycomb carbon: A review of graphene. *Chem. Rev.* **2010**, *110*, 132–145.

[47] Han, T. H.; Kim, H.; Kwon, S. J.; Lee, T. W. Graphene-based flexible electronic devices. *Mat. Sci. Eng. R.* **2017**, *118*, 1–43.

[48] Zheng, Q. B.; Li, Z. G.; Yang, J. H.; Kim, J. K. Graphene oxide-based transparent conductive films. *Prog. Mater. Sci.* **2014**, *64*, 200–247.

[49] Sahoo, N. G.; Pan, Y. Z.; Li, L.; Chan, S. H. Graphene-based materials for energy conversion. *Adv. Mater.* **2012**, *24*, 4203–4210.

[50] Han, S.; Wu, D. Q.; Li, S.; Zhang, F.; Feng, X. L. Porous graphene materials for advanced electrochemical energy storage and conversion devices. *Adv. Mater.* **2014**, *26*, 849–864.

[51] Gao, H. C.; Duan, H. W. 2D and 3D graphene materials: Preparation and bioelectrochemical applications. *Biosens. Bioelectron.* **2015**, *65*, 404–419.

[52] Kim, S. J.; Choi, K.; Lee, B.; Kim, Y.; Hong, B. H. Materials for flexible, stretchable electronics: Graphene and 2D materials. *Annu. Rev. Mater. Res.* **2015**, *45*, 63–84.

[53] Wang, Z. F.; Huang, Y.; Sun, J. F.; Huang, Y.; Hu, H.; Jiang, R. J.; Gai, W. M.; Li, G. M.; Zhi, C. Y. Polyurethane/cotton/carbon nanotubes core-spun yarn as high reliability stretchable strain sensor for human motion detection. *ACS Appl*. *Mater*. *Interfaces* **2016**, *8*, 24837–24843.

[54] Bae, G. Y.; Pak, S. W.; Kim, D.; Lee, G.; Kim, D. H.; Chung, Y.; Cho, K. Linearly and highly pressure-sensitive electronic skin based on a bioinspired hierarchical structural array. *Adv*. *Mater*. **2016**, *28*, 5300–5306.

[55] Chun, S.; Hong, A.; Choi, Y.; Ha, C.; Park, W. A tactile sensor using a conductive graphene-sponge composite. *Nanoscale* **2016**, *8*, 9185–9192.

[56] Zhang, H.; Zhang, Y.; Wang, B.; Chen, Z.; Sui, Y.; Zhang, Y.; Tang, C.; Zhu, B.; Xie, X.; Yu, G. et al. Effect of hydrogen in size-limited growth of graphene by atmospheric pressure chemical vapor deposition. *J. Electron. Mater*. **2015**, *44*, 79–86.

[57] Yu, Q. K.; Jauregui, L. A.; Wu, W.; Colby, R.; Tian, J. F.; Su, Z. H.; Cao, H. L.; Liu, Z. H.; Pandey, D.; Wei, D. G. et al. Control and characterization of individual grains and grain boundaries in graphene grown by chemical vapour deposition. *Nat*. *Mater*. **2011**, *10*, 443–449.

[58] Artyukhov, V. I.; Liu, Y.; Yakobson, B. I. Equilibrium at the edge and atomistic mechanisms of graphene growth. *Proc*. *Natl*. *Acad*. *Sci*. *USA* **2012**, *109*, 15136–15140.

[59] Li, X. S.; Magnuson, C. W.; Venugopal, A.; Tromp, R. M.; Hannon, J. B.; Vogel, E. M.; Colombo, L.; Ruoff, R. S. Large-area graphene single crystals grown by low-pressure chemical vapor deposition of methane on copper. *J. Am*. *Chem*. *Soc*. **2011**, *133*, 2816–2819.